



RESEARCH ARTICLE | DECEMBER 20 2024

## Fabricating distributed feedback laser gratings with bismuth and gold focused ion beams

Special Collection: [Papers from the 67th International Conference on Electron, Ion and Photon Beam Technology and Nanofabrication \(EIPBN 2024\)](#)

B. Salmond ; D. D. John ; W. J. Mitchell ; B. J. Thibeault ; T. Richter ; A. Nadzeyka ; P. Mazarov ; F. Meyer; J. Fridmann ; Y. Yu ; M. Wale ; W. Meredith; P. M. Smowton ; D. Read ; S. Shutts



*J. Vac. Sci. Technol. B* 42, 062214 (2024)

<https://doi.org/10.1116/6.0004056>



### Articles You May Be Interested In

Focused ion beams from GaBiLi liquid metal alloy ion sources for nanofabrication and ion imaging

*J. Vac. Sci. Technol. B* (October 2023)

Boron liquid metal alloy ion sources for special focused ion beam applications

*J. Vac. Sci. Technol. B* (May 2020)

Lithium ion beams from liquid metal alloy ion sources

*J. Vac. Sci. Technol. B* (March 2019)

## Instruments for Advanced Science


- Knowledge
- Experience
- Expertise

Click to view our product catalogue

Contact Hiden Analytical for further details:

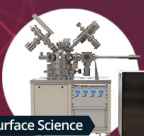
[www.HidenAnalytical.com](http://www.HidenAnalytical.com)

[info@hiden.co.uk](mailto:info@hiden.co.uk)




**Gas Analysis**

- ▶ dynamic measurement of reaction gas streams
- ▶ catalysis and thermal analysis
- ▶ molecular beam studies
- ▶ dissolved species probes
- ▶ fermentation, environmental and ecological studies




**Surface Science**

- ▶ UHV TPD
- ▶ SIMS
- ▶ end point detection in ion beam etch
- ▶ elemental imaging - surface mapping



**Plasma Diagnostics**

- ▶ plasma source characterization
- ▶ etch and deposition process reaction kinetic studies
- ▶ analysis of neutral and radical species



**Vacuum Analysis**

- ▶ partial pressure measurement and control of process gases
- ▶ reactive sputter process control
- ▶ vacuum diagnostics
- ▶ vacuum coating process monitoring

# Fabricating distributed feedback laser gratings with bismuth and gold focused ion beams

Cite as: J. Vac. Sci. Technol. B 42, 062214 (2024); doi: 10.1116/6.0004056

Submitted: 6 September 2024 · Accepted: 2 December 2024 ·

Published Online: 20 December 2024



B. Salmond,<sup>1,a)</sup> D. D. John,<sup>2</sup> W. J. Mitchell,<sup>2</sup> B. J. Thibeault,<sup>2</sup> T. Richter,<sup>3</sup> A. Nadzeyka,<sup>3</sup> P. Mazarov,<sup>3</sup> F. Meyer,<sup>3</sup> J. Fridmann,<sup>3</sup> Y. Yu,<sup>3</sup> M. Wale,<sup>4</sup> W. Meredith,<sup>5</sup> P. M. Smowton,<sup>1</sup> D. Read,<sup>1,2</sup> and S. Shutts<sup>1</sup>

## AFFILIATIONS

<sup>1</sup>School of Physics and Astronomy, Cardiff University, The Parade, Cardiff CF24 3AA, United Kingdom

<sup>2</sup>Nanofabrication Facility, Department of Electrical and Computer Engineering, University of California, Santa Barbara, California, 93106

<sup>3</sup>Raith GmbH, Konrad-Adenauer-Allee 8, 44263 Dortmund, Germany

<sup>4</sup>Department of Electronic and Electrical Engineering, University College London, London WC1E 7JE, United Kingdom

<sup>5</sup>Compound Semiconductor Centre Ltd, St Mellons, Cardiff CF3 0LW, United Kingdom

**Note:** This paper is part of the Special Topic Collection: Papers from the 67th International Conference on Electron, Ion and Photon Beam Technology and Nanofabrication (EIPBN 2024).

<sup>a)</sup>Author to whom correspondence should be addressed: [salmondb@cardiff.ac.uk](mailto:salmondb@cardiff.ac.uk)

## ABSTRACT

Fabricating first order gratings for laterally coupled distributed feedback (LC-DFB) lasers can be challenging due to aspect ratio dependent etching. Developments in focused ion beam (FIB) processing and source technology introduce the potential to mill grating structures directly into a ridge waveguide (RWG) laser structure without the requirement for electron beam lithography and inductively coupled plasma etching. In this work, we investigate the suitability of using bismuth and gold FIBs to mill Bragg gratings for DFB laser diodes directly into as well as adjacent to InP RWG laser structures. We explore the milling strategy on the profile of the fabricated grating structures. We observe that the single pixel line scanning routine is favorable when milling directly onto an RWG and using a concentric scanning method is better when milling the grating structures adjacent to the RWG. We conclude that milling off-ridge is more promising using this technique, as gratings with sidewall angles of 18° have been milled to a depth of over 350 nm. Based on modeling, a grating milled adjacent to the ridge with a dose of 60 000  $\mu\text{C}/\text{cm}^2$  would provide a coupling strength of 73  $\text{cm}^{-1}$ . Such values would be suitable for DFB laser devices with cavity lengths as low as 200  $\mu\text{m}$ .

© 2024 Author(s). All article content, except where otherwise noted, is licensed under a Creative Commons Attribution (CC BY) license (<https://creativecommons.org/licenses/by/4.0/>). <https://doi.org/10.1116/6.0004056>

## I. INTRODUCTION

Distributed feedback (DFB) laser diodes are widely used in long range data communication systems owing to their ability to provide stable single mode emission and narrow linewidth.<sup>1</sup> They have also found a number of other uses including gas sensing,<sup>2</sup> LiDAR,<sup>3</sup> and medical applications.<sup>4</sup> In these devices, single mode emission is provided by a Bragg grating, which extends throughout the length of the laser located within the vicinity of the optical waveguide in laser active region.<sup>5</sup> In a conventional buried grating

DFB laser structure, the grating is defined by a two stage etch and epitaxial regrowth process. In this method, the lower epitaxial layers are grown first, followed usually by electron beam lithography (EBL) and etching of the grating. The upper epitaxial layers are then grown on top of the grating structure. Interrupting the growth process in this way can introduce defects into the structure and places stringent demands on cleanliness and surface preparation.<sup>6</sup> Despite these issues, regrowth processes are well established for large scale manufacturing of DFB-only wafers. They are, however, relatively incompatible when fabricating photonic

13 January 2025 14:24:23

integrated circuits (PICs), where multiple optical components are placed on the same chip.

Alternatively, DFB laser diodes can be fabricated in such a way that only a single growth and fabrication run is required to manufacture them. The most common type of single growth DFB laser is known as the laterally coupled DFB (LC-DFB) laser and is well established in the literature, having been presented for the first time in the 1990s.<sup>7</sup> In an LC-DFB laser, the gratings are placed on either side of the lasing stripe or ridge waveguide (RWG) and are often attached to the ridge such that only a single EBL and etch process is required to transfer the grating into the epitaxial structure. The etch process for this type of design is extremely challenging however, due to the phenomenon of aspect ratio dependent etching (ARDE).<sup>8</sup> This occurs due to the fact that the gaps in the grating structure for a c-band (1530–1565 nm) DFB laser diode based on InP are on the order of 100 nm. When the structure is etched, the etch products within the gaps are not removed as fast as the other, more open areas of the wafer, which results in a reduced etch depth in the grating gaps especially next to the RWG. In the LC-DFB grating structure, the portion of the grating closest to the bottom of the ridge is critical for achieving strong coupling of the grating to the optical mode. As such, a poor profile here results in poor single mode lasing performance. Previous works have circumvented this issue in a variety of ways. In many cases, higher order gratings are used. For example, a third order grating has a gap size on the order of 300 nm when targeting c-band emission. This reduces the severity of ARDE and has been applied in previous work to good effect.<sup>9</sup> Using a third order grating, however, introduces diffraction loss, resulting in a reduced coupling strength. In addition to this, the coupling strength of a third order grating is more sensitive to changes in the duty cycle, potentially reducing the device yield. Due to this, the grating either has to be made significantly larger than a first order grating to achieve the necessary coupling strength or the cavity length must be increased. This can negatively impact the device performance, particularly under direct modulation. Another method is to use deposited metal to form a gain-coupled grating<sup>10</sup> and while high coupling coefficients can be achieved, the introduction of metal close to the active region results in an additional source of loss.

In order to address the issues described above, it would be desirable to remove the etching step for the grating altogether. Focused ion beam (FIB) nanofabrication presents an opportunity to do this as it is a direct write technique. This means that the depth of the grating can be controlled separately from the depth of the RWG. This would be extremely difficult to achieve with an EBL +dry etch process, as it would require multiple lithography and etch steps. Furthermore, FIB can define patterns independently of other topography on the wafer. This means that structures can be designed where the grating no longer has to be attached to the ridge. Again, using the traditional EBL method, this would be extremely challenging as the thickness of resist spun on top of a ridge would be highly nonuniform especially close to the ridge, where the grating is located. In recent years, FIB milling has been used to fabricate a wide variety of optical structures including photonic crystals and other photonic components.<sup>11,12</sup> In all these examples, the structures have been milled over a small area in a single write field. This is not suitable for defining a grating across a

whole cavity length for a laser diode, which can be on the order of 200–1000  $\mu\text{m}$ . Additionally, the use of a traditional gallium FIB system is not suitable for large areas for two reasons; the first is that patterning times are significantly longer than other high-resolution techniques. The second is that these systems tend to be designed primarily as metrology tools and, therefore, do not offer large writefields or stitching, which is essential for the patterning of larger areas. Recent advances in FIB nanofabrication have introduced top-down FIB geometries with laser interferometer stages.<sup>13</sup> This facilitates writefields as wide as  $200 \times 200 \mu\text{m}$  with the ability to perform stitching for patterning multiple writefields. Furthermore, developments in liquid metal alloy ion source (LMAIS) technology have introduced the ability to mill with heavy ions such as bismuth and gold, which decrease the patterning time compared to traditional gallium as a result of a higher sputter yield.<sup>14</sup>

In this work, we explore the possibility of fabricating laterally coupled grating structures with bismuth and gold FIB lithography. Two different designs are presented and the suitability of different milling routines is examined through a combination of scanning electron microscopy (SEM) and FIB cross sectioning.

## II. METHODOLOGY

### A. Ridge waveguide preparation

All structures in this work were fabricated on an InP-based epitaxial structure with a separate confinement heterostructure (SCH) including multiple AlGaInAs quantum wells. The SCH is contained within two  $1.5 \mu\text{m}$  InP cladding layers with a 150 nm thick highly doped InGaAs capping layer on top of the structure. The ridge waveguide was defined by first depositing a 400 nm silicon dioxide hard mask. This was subsequently patterned using projection lithography (Heidelberg MLA150) on negative tone photoresist. Two ICP-RIE etching steps were then used to transfer the RWGs first to the oxide and second to the epitaxial structure. The RWGs were etched to a target depth of  $1.5 \mu\text{m}$  and a number of ridge widths were included in the design ranging from 1.5 to  $4 \mu\text{m}$ .

Following the fabrication of the RWG laser structures, FIB milling was used to directly mill the gratings into the structure. The gratings were milled either into the ridge itself, which we define as an “on-ridge” grating [Fig. 1(a)] or adjacent to the ridge, which we refer to as an “off-ridge” grating [Fig. 1(b)]. In order to assess the quality of the grating structures for a large range of FIB scanning routines, test structures were milled. These included 20 periods of each grating type, which had a pitch of 238 nm designed for emission in the c-band at 1550 nm. The two designs considered in this work are shown in Fig. 1. In order to examine these gratings, SEM imaging was used to measure the grating dimensions and in some cases gratings were cross sectioned using FIB and subsequently imaged using SEM. Dimensions were measured at multiple locations for each structure and we have taken the standard deviation in these measurements to represent the uncertainty. To ensure that reliable information was gained from the FIB cross sections, platinum was deposited on the structure of interest prior to milling a deep trench to reveal the sub-surface information. The deposition of platinum using the gas injection system limits the effects of redeposition and curtaining and, therefore, limits the extent to which the milled structure is altered by the cross sectioning process.<sup>15</sup>

13 January 2025 14:24:23

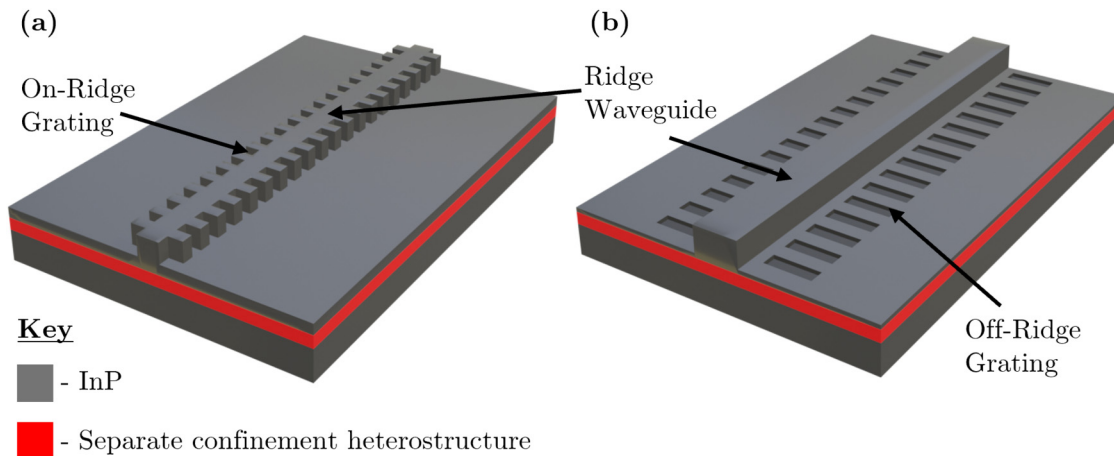


**FIG. 1.** Schematics of the two LC-DFB laser designs fabricated in this work. (a) “On-ridge” grating structure. (b) “Off-ridge” grating structure.

Once the methods described above had revealed the necessary dimensions, the devices were modeled by adapting the methodology described by Laakso *et al.*<sup>16</sup> This work provided the coupling strength,  $\kappa$ , which is a measure of how well the optical mode is coupled to the grating region in a device. It is generally accepted that a value of between  $\kappa L = 1.5$  and  $\kappa L = 2.5$  is desirable, where  $L$  represents the grating length.

### B. Focused ion beam system and milling strategy

All of the FIB milling described in this work was performed using a Raith Velion FIB-SEM. In a traditional FIB-SEM, which typically have a top-down SEM column with the FIB column at an angle, the sample stage is tilted depending on whether milling or imaging is taking place. The disadvantage to this is that only single write fields can be used. The system used in this work uses a top-down FIB geometry with an angled SEM. This facilitates high-resolution milling over large write fields up to  $200 \times 200 \mu\text{m}$ . Additionally, the Raith Velion is fitted with a laser interferometer stage, which allows the possibility of patterning multiple write fields with stitching. In addition to this, the laser interferometer stage can facilitate a fixed beam moving stage mode, where patterning can be performed over several millimeters without the need for stitching. The system used in this work had an accelerating voltage of 35 kV and all the patterning discussed here was performed with a beam current of 30 pA. Increasing this further would decrease the dwell time (the time the beam spends exposing a single pixel), however, this current was found to provide the best balance between patterning time and the amount of damage caused to the regions surrounding the milled area. All test structures were fabricated using a  $40 \times 40 \mu\text{m}$  writefield with a beam step size of 5 nm. Milling was performed using both bismuth and gold ions, which according to the literature have similar minimum trench widths of around 60 nm.<sup>14</sup>

In contrast to other forms of direct write lithography, patterning with the FIB offers many scanning routines which influence

both the profile and milling rate markedly. We have examined the use of two different types of scanning routine, namely, single pixel line (SPL) scans and area scans. The SPL method is the simplest as the only considerations in the grating design process are the length of the SPLs and the pitch. An important consideration is the direction the line is scanned in, which as will be shown below, has a considerable effect on the profile of the milled trench. The second type of scanning routine used in this work is known as area scanning. This simply means that the designed shapes are two-dimensional rather than one-dimensional. The area scans investigated in this work can be separated into two categories, longitudinal and concentric. Longitudinal scanning separates the designed shape into a series of lines, which are then scanned in the direction of the longest axis of the shape. Once again, the direction the lines are scanned in can be varied both across shapes and within a shape itself. Concentric scanning scans the shapes in a circular fashion either from inside out or outside in. The scanning routines used in this work are illustrated in Fig. 2.

Among all the scanning routines described here, the number of times a pixel or beam shot is addressed in the patterning process can be altered. The parameter that determines this is often referred to as “loops.” In other words, a single loop scan means that the full dose is provided to each pixel sequentially. When the number of loops is increased, the dose is distributed over the number of loops selected i.e., on each loop a single pixel receives  $1/n \times \text{dose}$  where  $n$  is the number of loops. It is well established that increasing the number of loops results in a reduced redeposition effect, which is where material that is being milled is immediately deposited onto regions that were previously milled. This effect is usually not desired as it affects the uniformity in the profile of a milled shape.<sup>17</sup>

### III. ON-RIDGE GRATING MILLING

We describe first the on-ridge patterning of first order gratings directly into the RWG laser structure. The required milling depth here was  $1.6 \mu\text{m}$ , which was the depth of the ridge. A milling depth

13 January 2025 14:24:23

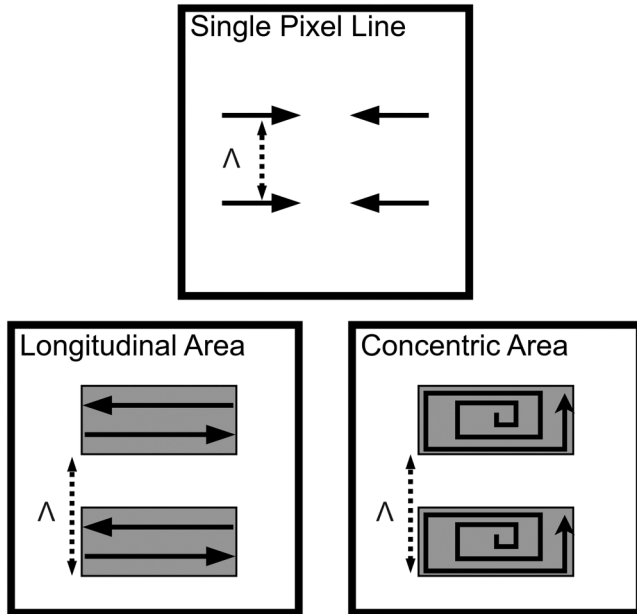


FIG. 2. Three scanning routines used in this work. The solid arrows indicate the movement of the FIB and the grating pitch,  $\Lambda$ , is indicated by the dotted arrows.

significantly less than this would result in inadequate coupling of the optical mode to the grating and as such poor single mode performance in a completed device. Milling too far would expose the aluminum containing active region and increase optical loss in the device. We refer to the length that the grating extrudes from the RWG as the extrusion length. This parameter can be altered depending on the required coupling strength for the grating. In this case, we have designed the gratings with extrusion lengths of  $0.5\text{--}1\ \mu\text{m}$  and a duty cycle of 0.5. The use of the area scanning routine was found to cause significant damage to the ridge and grating structure; therefore, only the results of the SPL scanning routine will be described for the on-ridge grating structures.

### A. Single pixel line scanning routine for on-ridge gratings

Figure 3 shows the results of using the SPL scanning routine to mill the on-ridge gratings. Figure 3(a) shows an SPL scan where a dose of  $158.4\ \text{nC/cm}$  and a pixel dwell time of 3 ms per pixel was used. Additionally, the scanning direction used here started on the exterior of the ridge and moved toward the interior. Milling against the topography in this way reduces the required dose due to the fact that sputter yield increases with incidence angle.<sup>18</sup> The result of this is a reduced patterning time and so this was selected as the default for SPL scanning. Using this method, the grating appears exhibit a teardrop shape, with the wider section appearing at the interior of the grating. We attribute this profile to the redeposition effect, which is more pronounced due to the fact that only a single loop has been used here. The interior section of the grating was

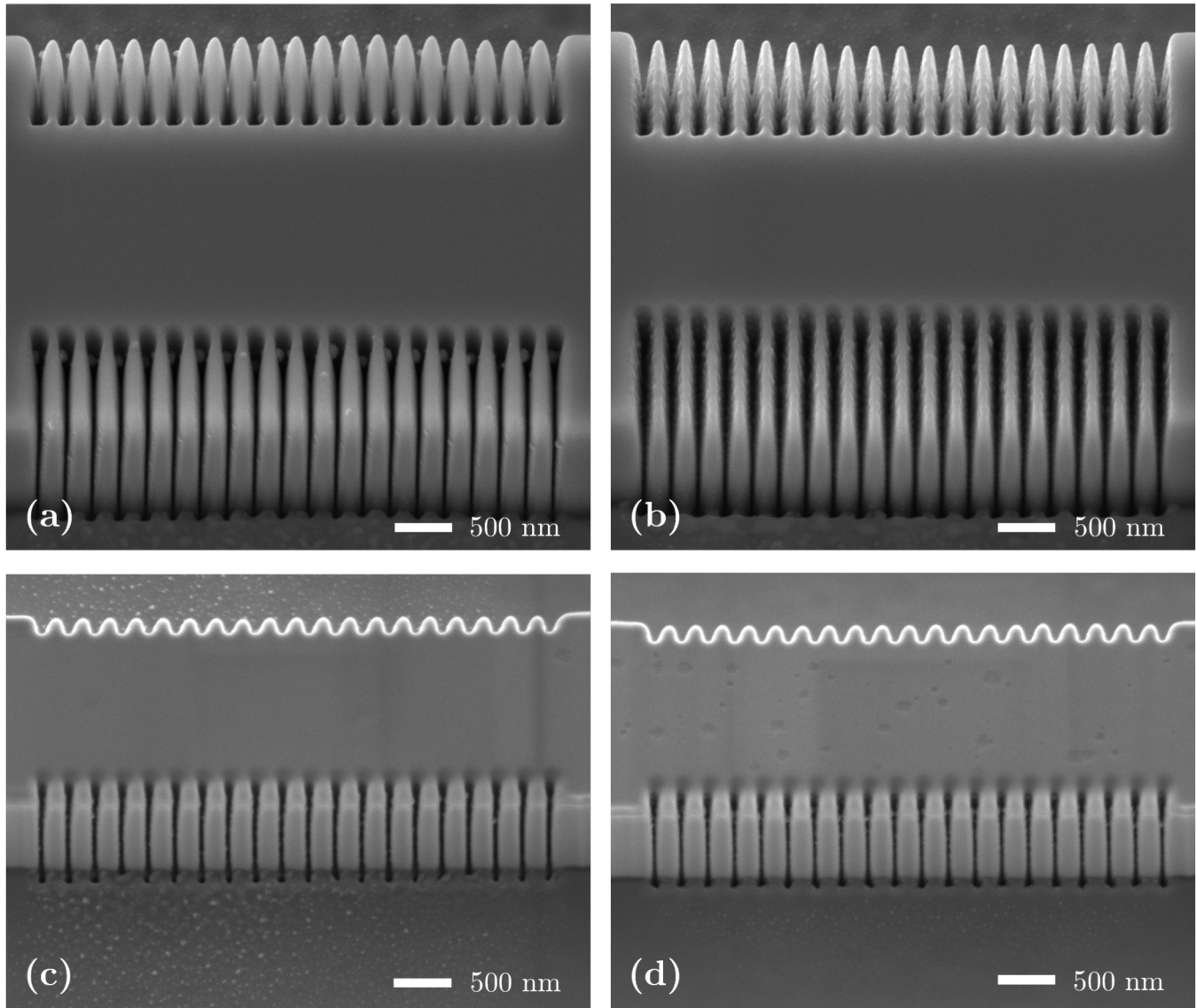
wider since this was patterned last and, therefore, experienced less redeposition. Top-down SEM imagery was used to measure the pitch, which was found to be  $(239 \pm 5)\ \text{nm}$ , and gap size of the grating which was found to be  $(22 \pm 5)\ \text{nm}$  at its narrowest point and  $(115 \pm 7)\ \text{nm}$  at its widest point. The gap size being as narrow as 22 nm reinforces the idea that the effect of redeposition is strong when a single loop is used. Figure 3(b) shows the same design of the ridge grating; however, this time 1000 loops were used with a dose of  $264\ \text{nC/cm}$  and a dwell time of  $5\ \mu\text{s}$  per pixel per loop. The higher dose was required to mill the gratings into the ridge fully, which suggests that increasing the number of loops decreases the milling efficiency to a certain extent. This may be caused by the fact that this type of scan does not benefit from the increased milling rate when milling against the topography as the beam is scanned in alternate directions on each loop. From Fig. 3(b), it can be seen that increasing the number of loops has resulted in greater uniformity in the gap size at the top surface of the grating structure. The pitch was measured to be  $(239 \pm 7)\ \text{nm}$  in this case and the gap size at the top surface of the grating was  $(128 \pm 7)\ \text{nm}$ , which is closer to the desired value of 119 nm, corresponding to a duty cycle of 0.5. It is clear from Fig. 3 that in both cases where an SPL scanning routine has been used the grating gap size does not widen to the same extent as the top. Once again this effect can be explained by redeposition, which ensures that the higher the aspect ratio of the milled structure, the less material will be removed from the milled area causing the structure to narrow at the bottom.

Using Au ions to mill on-ridge gratings shows similar results. Figure 3(c) shows an on-ridge grating milled using gold ions where a single loop SPL line scan has been used at a dose of  $150\ \text{nC/cm}$ . For this grating, the pitch was measured to be  $(236 \pm 5)\ \text{nm}$  and the gap size at the narrowest and widest point were measured to be  $(21 \pm 5)\ \text{nm}$  and  $(66 \pm 7)\ \text{nm}$ , respectively, at the top of the grating structure. The gap size at the bottom of the RWG was measured to be  $(37 \pm 5)\ \text{nm}$ . This was notably wider than found in Fig. 3(a). We attribute this to the fact that the ridge itself was not etched as deep at a depth of approximately  $1.3\ \mu\text{m}$ , since when a single loop is used, a milled trench becomes narrower the deeper it is milled.<sup>19</sup> The fact that the same dose was required for less milled depth in the case of the gold ions is attributed to the fact that the sputter yield of gold is slightly less than that of bismuth. Figure 3(d) shows the same design where 1000 loops have been used at the same dose. Once again, although it appears the gratings have been broadened on the top surface of the RWG, at the bottom of the structure the grating gap size is  $(28 \pm 5)\ \text{nm}$ , which is narrower than where a single loop is used. This reinforces the possibility that for high aspect ratio structures such as these, increasing the number of loops does not necessarily improve the effect of redeposition, especially at the bottom of the grating structure.

### B. Cross sections of on-ridge gratings

In an on-ridge LC-DFB structure, the interior portion of the grating interacts most with the optical mode. As such, the profile here is important for achieving good coupling. In order to assess the profile of the gratings at the interior of the grating, cross sections were made in gratings milled using gold ions for both a single loop and 1000 loops. The dose in each case was chosen such that

13 January 2025 14:24:23



13 January 2025 14:24:23

**FIG. 3.** On-ridge gratings milled using the single pixel line scanning routine and (a) bismuth ions with one loop at a dose of 158.4 nC/cm, (b) bismuth ions with 1000 loops at a dose of 264 nC/cm, (c) gold ions with one loop at a dose of 150 nC/cm, and (d) gold ions with 1000 loops at a dose of 250 nC/cm. (a) and (b) are shown on a ridge with a width of 4  $\mu\text{m}$  and (c) and (d) are shown on a ridge with width 2  $\mu\text{m}$ .

the grating was milled completely through an RWG structure at a depth of 1.6  $\mu\text{m}$ . In both cases, the interior of the grating structures was not milled through the full depth of the ridge. Figure 4 shows an example of this where a dose of 400 nC/cm and 1000 loops has been used. In this case, the gratings have been milled to a depth of  $(786 \pm 9)$  nm. When a single loop is used with a dose of 300 nC/cm, the milled depth reached  $(1078 \pm 16)$  nm. This suggests that using a single loop SPL scanning routine is the most efficient way to mill these on-ridge grating structures as a higher depth has been achieved with less dose. However, additional optimization is

required to achieve milling through the whole depth of the structure. One way to achieve this may be to use a graded dose technique where the interior of the grating structure receives a higher dose than the exterior.

#### IV. OFF-RIDGE GRATING MILLING

Next we describe the development of the off-ridge grating structure presented in Fig. 1(b). This structure should in theory be simpler to mill as the depth required is much less than the on-ridge grating structures presented in Sec. III. Such a structure

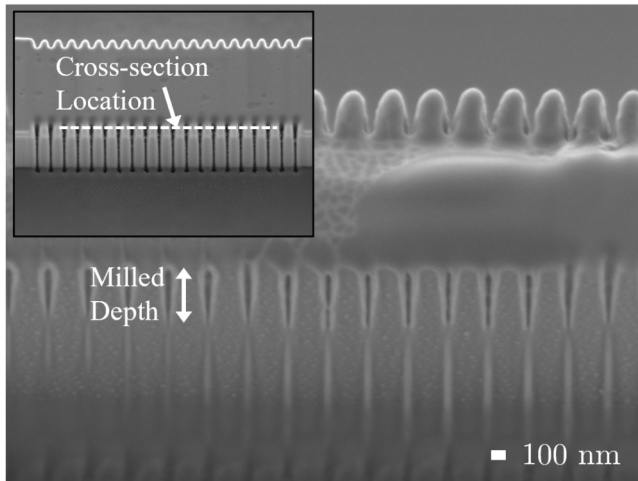
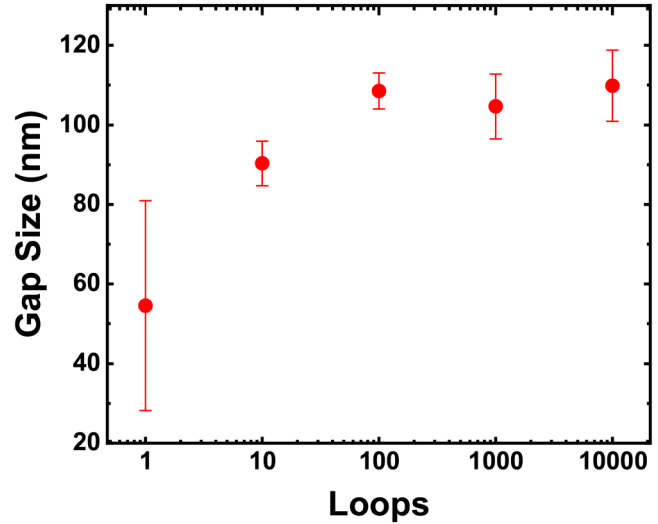
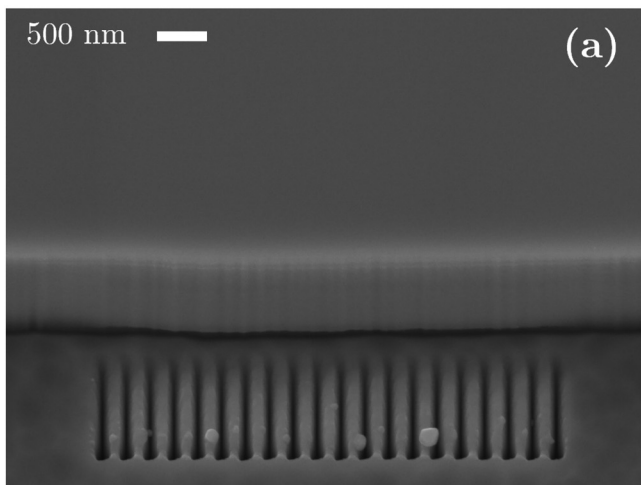


**FIG. 4.** On-ridge gratings milled using gold ions using the single pixel line scanning routine and subsequently cross sectioned using the FIB. The dose was 400 nC/cm with 1000 loops. Milled depth is shown and the inset shows an overview of the grating with a dashed line indicating where the cross section was made.

would also be extremely difficult to produce using a conventional electron beam lithography and etch process, likely involving multiple masking and etch steps. Here, we use the fact that using FIB nanofabrication we can define these structures independent of the topography of the sample.

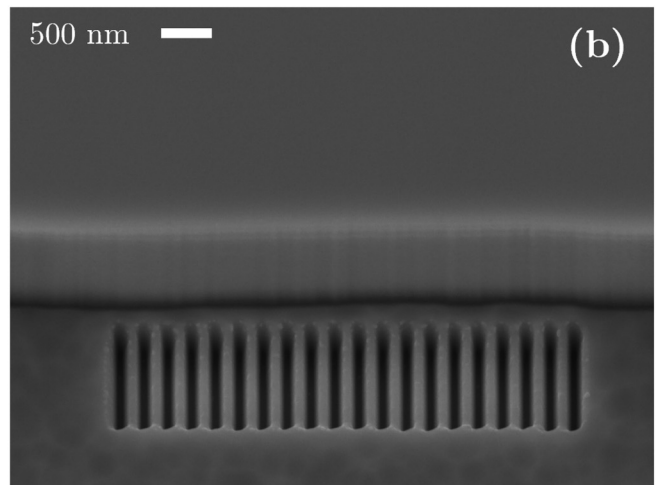
#### A. Single pixel line scanning routine for off-ridge gratings

Figure 5 shows the SPL scanning routine results for the off-ridge gratings structure milled with bismuth ions. Figure 5(a)



**FIG. 6.** Grating gap size as a function of loops for off-ridge gratings milled using the SPL scanning routine with a dose of 150 nC/cm.

shows a SPL scan at a dose of 158 nC/cm and a dwell time of 2.6 ms, where a single loop has been used. Similarly to the on-ridge grating results, it is observed that the width of the grating gaps is variable across the milled region. This structure was milled in the direction moving away from the ridge. Therefore, the widest point is farthest away from the ridge because this area suffers least from the redeposition effect. In this case, the width at the narrowest point was measured to be  $(27 \pm 5)$  nm and  $(111 \pm 5)$  nm at the widest point. Additionally, large particles of redeposited material are visible on the surface of the milled area. Figure 5(b) shows an off-ridge grating structure milled with a dose of 264 nC/cm, 1000



**FIG. 5.** Off-ridge grating structures milled with the SPL scanning routine and (a) one loop at a dose of 150 nC/cm and (b) 1000 loops at a dose of 264 nC/cm.

13 January 2025 14:24:23

loops, and a dwell time of  $4.4\mu\text{s}$ . Here, greater uniformity in the gap size is observed, and it appears that the gap size has widened significantly. Furthermore, the large particles observed in Fig. 5(a) are not observed in Fig. 5(b). We attribute this to the redeposition effect, which is mitigated by the increased number of loops. Where a single loop is used, large particles are ejected from the material as higher dose is applied per pixel. Although not shown, the same effect was observed when milling was performed using gold ions. In order to investigate whether control over duty cycle was achievable by altering the dose, a series of test structure using identical dose and varying loops was milled using gold ions. Using SEM, the gap size in the gratings was measured as a function of dose. This is shown in Fig. 6. As the number of loops increases so does the gap size. This is the trend to around 100 loops beyond which increasing the loops does little to affect the gap size. This demonstrates that a degree of control over the duty cycle is achievable by changing the number of loops. Specifically, the duty cycle on the top surface of the grating can be varied from around 0.55 to 0.8 using this technique. Additionally, we observed a higher degree of variability in the gap size where a single loop has been used. This is a result of the redeposition effect, which results in a wider gap size at the end of the FIB movement, as shown in Fig. 5(a).

### B. Area scanning routine for off-ridge gratings

Next, we consider the area scanning routine. Figure 7 shows an off-ridge grating that has been scanned using a longitudinal scanning routine with 1000 loops at a dose of  $52\,800\mu\text{C}/\text{cm}^2$ . In this case, the dwell time was  $0.5\mu\text{s}$  per pixel per loop. Each gap was designed at  $50\text{ nm}$  in width and the actual measured size of the gaps at the top of the grating structure was measured to be  $(153 \pm 11)\text{ nm}$ . This corresponds to a duty cycle of 0.46 and so indicates that more control over the duty cycle may be possible using the area scanning routine.

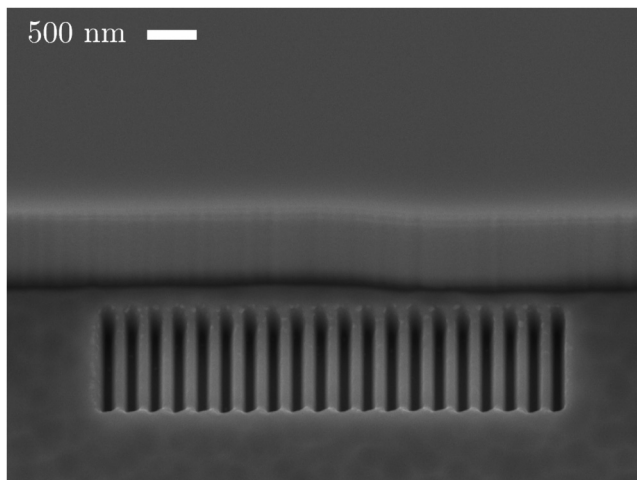


**FIG. 7.** Off-ridge grating that has been milled using bismuth ions and a longitudinal scanning routine with a dose of  $52\,800\mu\text{C}/\text{cm}^2$ .

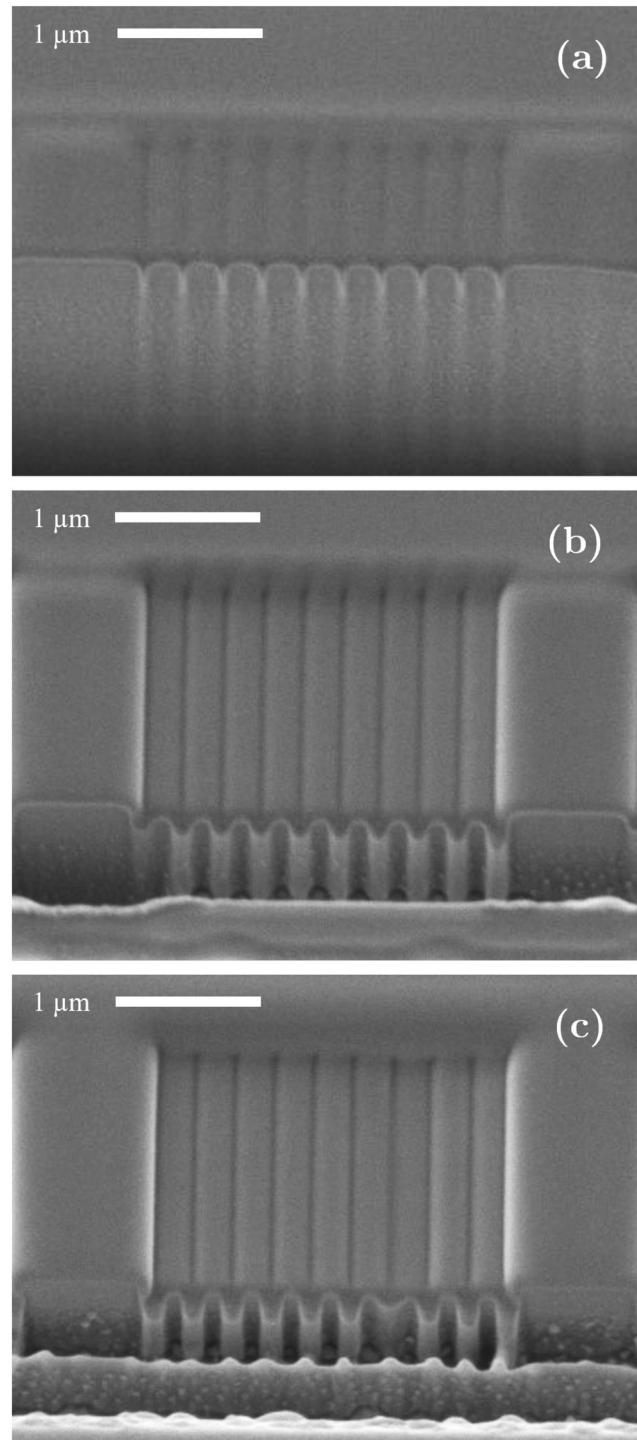


**FIG. 8.** Cross sections of off-ridge grating test structures using (a) SPL scanning routine with a dose of  $120\text{ nC}/\text{cm}$ , (b) longitudinal scanning routine with a dose of  $120\,000\mu\text{C}/\text{cm}^2$ , and (c) concentric scanning routine with a dose of  $120\,000\mu\text{C}/\text{cm}^2$ .

13 January 2025 14:24:23



### C. Cross sections of off-ridge gratings

In order to make an informed estimate of the coupling strength of our fabricated gratings, it was necessary to know the profile and the depth at which the gratings are milled. A series of test gratings were milled using gold ions with various doses and scanning routines and cross sectioned using the procedure described earlier. Examples of these cross sections are shown in Fig. 8. Figure 8(a) shows a cross section of a grating milled using the SPL scanning routine with a dose of 120 nC/cm. This grating was measured to have a milled depth of  $(432 \pm 9)$  nm. However, the duty cycle is not uniform across the depth of the structure. Specifically, the gap size at the top of the grating structure was measured to be  $(102 \pm 9)$  nm while the width at the bottom of the structure was measured to be  $(54 \pm 5)$  nm. These values correspond to a duty cycle of 0.55 and 0.77 at the top and bottom of the structure, respectively, and exceed the targeted value of 0.5. Having high duty cycle in this way actually increases the coupling strength which may positively impact device performance. From a purely visual standpoint, using area scanning routines appeared to deliver more desirable profiles. Figures 8(b) and 8(c) show gratings milled with a dose of  $120\,000\ \mu\text{C}/\text{cm}^2$  using gold ions and the longitudinal and concentric scanning routines, respectively. In both cases, the width of each milled section of the grating was designed at 50 nm, the number of loops was 100, and the dwell time was  $10\ \mu\text{s}$  per pixel per loop. The gratings milled using the longitudinal scanning routine [Fig. 8(b)] are measured to be a depth of  $(280 \pm 4)$  nm, and the grating milled using the concentric scanning routine [Fig. 8(c)] is measured to be a depth of  $(378 \pm 5)$  nm. Additionally, the sidewall angle was measured to be more vertical when using the concentric scanning routine at  $18^\circ$  than the longitudinal scanning routine which was measured at  $30^\circ$ . In order to

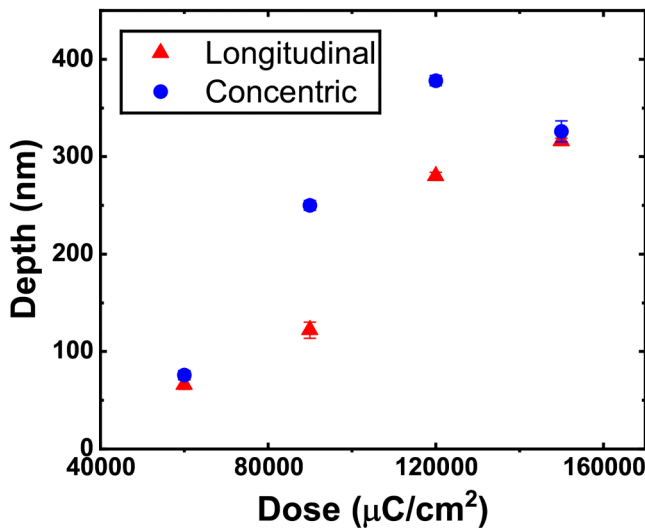


FIG. 9. Depth as a function of dose for off-ridge grating structures milled using gold ions with the longitudinal (triangle) and concentric (circles) scanning routines.

compare the two methods further, we milled a series of test structures at different doses ranging from 15 000 to  $150\,000\ \mu\text{C}/\text{cm}^2$ . The results of this test are shown in Fig. 9. Here, we observe that a range of depths can be achieved from less than 100 to over 300 nm. It is worth noting that smaller depths may be achievable; however, the test grating milled with doses lower than  $60\,000\ \mu\text{C}/\text{cm}^2$  was unresolvable most likely due to the cross-sectioning procedure. We also observed that at higher doses the depth of the milled structure appears to decrease. This is attributed to increased milling of the surrounding area, which reduces the height of the whole structure. The results shown in Fig. 9 suggest that the concentric area scanning routine is more efficient in the milling of the off-ridge grating structures, as with the same dose, a higher depth is achieved compared to the longitudinal scanning routine. This is in contrast to the on-ridge grating structures, where the SPL scanning routine was found to be more effective. Based on the modeling techniques described earlier in this work, we estimated the coupling coefficient of the test grating milled using the concentric area scanning routine with a dose of  $60\,000\ \mu\text{C}/\text{cm}^2$ . For this calculation, we assume that the RWG is  $2\ \mu\text{m}$  wide, is etched to a depth of  $1.5\ \mu\text{m}$ , and the grating is located 100 nm away from the side of the RWG. With these assumptions, the coupling coefficient would be  $73\ \text{cm}^{-1}$ . This value would provide the appropriate coupling strength for lasers with cavity lengths as low as  $200\ \mu\text{m}$  with a target of  $\kappa L = 1.5$ .

### V. CONCLUSIONS

Recent advances in FIB nanofabrication systems have introduced the ability to directly mill patterns over wide writefields with heavier ions than traditional gallium. We have demonstrated the potential for using bismuth and gold FIBs to define grating structures on RWG laser structures in InP epitaxial structures. Two structures have been fabricated; both an on-ridge grating where the periodic structure is milled directly into the ridge waveguide and an off-ridge grating where the structure is milled into the etched area adjacent to the waveguide.

For the on-ridge gratings, we have compared the effect of varying the number of loops in the single pixel line scanning routine and found that it was more efficient to use a single loop due to the fact that more efficient milling was achieved. Further optimization is required, however, as the achieving milling through the full depth of the ridge was challenging due to the redeposition effect, which is exacerbated by the high aspect ratio nature of these structures.

For the off-ridge gratings, a variety of scanning routines were compared, including SPL, longitudinal scans, and concentric scans. We found that concentric scanning offered the most desirable profile, achieving a grating that was measured to be 76 nm deep with an estimated coupling strength of  $73\ \text{cm}^{-1}$  for a milling dose of  $60\,000\ \mu\text{C}/\text{cm}^2$ . Based on this value for coupling strength, this grating should provide adequate coupling for cavity lengths as low as  $200\ \mu\text{m}$ . We believe this technique would be particularly advantageous for PICs as the grating fabrication could be performed later in the process after the definition of other optical components. Furthermore, this method could be extended to other photonic structures such as grating couplers or DBR mirrors.

13 January 2025 14:24:23

## ACKNOWLEDGMENTS

This work was supported by the Taith research mobility program, the UKRI Strength in Places Fund (Grant No. 107134) and the Engineering and Physical Sciences Research Council (Grant No. EP S024441/1). A portion of this work was performed in the UCSB Nanofabrication Facility, an open access laboratory. The ridge waveguide fabrication was carried out in the cleanroom of the Institute for Compound Semiconductors (ICS) at Cardiff University.

## AUTHOR DECLARATIONS

### Conflict of Interest

The authors have no conflicts to disclose.

### Author Contributions

**B. Salmond:** Conceptualization (equal); Data curation (equal); Formal analysis (equal); Investigation (equal); Methodology (equal); Validation (equal); Visualization (equal); Writing – original draft (equal); Writing – review & editing (equal). **D. D. John:** Conceptualization (equal); Writing – review & editing (equal). **W. J. Mitchell:** Conceptualization (equal); Writing – review & editing (equal). **B. J. Thibeault:** Conceptualization (equal); Resources (equal); Writing – review & editing (equal). **T. Richter:** Resources (equal); Writing – review & editing (equal). **A. Nadzeyka:** Resources (equal); Writing – review & editing (equal). **P. Mazarov:** Resources (equal); Writing – review & editing (equal). **F. Meyer:** Resources (equal); Writing – review & editing (equal). **J. Fridmann:** Resources (equal); Writing – review & editing (equal). **Y. Yu:** Resources (equal); Writing – review & editing (equal). **M. Wale:** Supervision (equal); Writing – review & editing (equal). **W. Meredith:** Resources (equal); Supervision (equal); Writing – review & editing (equal). **P. M. Smowton:** Funding acquisition (equal); Writing – review & editing (equal). **D. Read:** Conceptualization (equal); Data curation (supporting); Formal analysis (supporting); Investigation (supporting); Methodology (equal); Resources (equal); Validation (equal); Writing – review & editing (equal). **S. Shutts:** Conceptualization (equal); Funding

acquisition (equal); Project administration (lead); Supervision (equal); Writing – review & editing (equal).

## DATA AVAILABILITY

The data that support the findings of this study are available from the corresponding author upon reasonable request.

## REFERENCES

- <sup>1</sup>J. E. Carroll, J. Whiteaway, and D. Plumb, *Distributed Feedback Semiconductor Lasers*, SPIE Press Monograph No. 52 (Institution of Electrical Engineers SPIE Optical Engineering, London, 1998).
- <sup>2</sup>V. Weldon, J. O’Gorman, P. Phelan, J. Hegarty, and T. Tanbun-Ek, *Sens. Actuators, B* **29**, 101 (1995).
- <sup>3</sup>X. Zhang, J. Pouls, and M. C. Wu, *Opt. Express* **27**, 9965 (2019).
- <sup>4</sup>D. E. Cooper, R. U. Martinelli, C. B. Carlisle, H. Riris, D. B. Bour, and R. J. Menna, *Appl. Opt.* **32**, 6727 (1993).
- <sup>5</sup>H. Kogelnik and C. V. Shank, *J. Appl. Phys.* **43**, 2327 (1972).
- <sup>6</sup>S. Chu, T. Tanbun-Ek, A. Logan, J. Vandenberg, P. Sciortino, P. Wisk, and T. Pernell, *IEEE J. Sel. Top. Quantum Electron.* **3**, 862 (1997).
- <sup>7</sup>L. Miller, J. Verdeyen, J. Coleman, R. Bryan, J. Alwan, K. Beernink, J. Hughes, and T. Cockerill, *IEEE Photonics Technol. Lett.* **3**, 6 (1991).
- <sup>8</sup>R. A. Gottscho, C. W. Jurgensen, and D. J. Vitkavage, *J. Vac. Sci. Technol. B* **10**, 2133 (1992).
- <sup>9</sup>K. Dridi, A. Benhsaien, J. Zhang, and T. J. Hall, *IEEE Photonics Technol. Lett.* **26**, 1192 (2014).
- <sup>10</sup>S. J. Jang, J. S. Yu, and Y. T. Lee, *IEEE Photonics Technol. Lett.* **20**, 514 (2008).
- <sup>11</sup>W. C. L. Hopman, F. Ay, W. Hu, V. J. Gadgil, L. Kuipers, M. Pollnau, and R. M. D. Ridder, *Nanotechnology* **18**, 195305 (2007).
- <sup>12</sup>P. M. Nellen and R. Brönnimann, *Meas. Sci. Technol.* **17**, 943 (2006).
- <sup>13</sup>T. Richter, A. Nadzeyka, P. Mazarov, and F. Meyer, *Microsc. Microanal.* **29**, 536 (2023).
- <sup>14</sup>L. Bischoff, P. Mazarov, L. Bruchhaus, and J. Gierak, *Appl. Phys. Rev.* **3**, 021101 (2016).
- <sup>15</sup>L. A. Giannuzzi and F. A. Stevie, *Micron* **30**, 197 (1999).
- <sup>16</sup>A. Laakso, M. Dumitrescu, J. Viheriälä, J. Karinen, M. Suominen, and M. Pessa, *Opt. Quantum Electron.* **40**, 907 (2008).
- <sup>17</sup>H. Yamaguchi, A. Shimase, S. Haraichi, and T. Miyauchi, *J. Vac. Sci. Technol. B* **3**, 71 (1985).
- <sup>18</sup>L. Frey, C. Lehrer, and H. Rysse, *Appl. Phys. A* **76**, 1017 (2003).
- <sup>19</sup>H.-W. Li, D.-J. Kang, M. G. Blamire, and W. T. S. Huck, *Nanotechnology* **14**, 220 (2003).

13 January 2025 14:24:23